THE JOURNAL OF BIOLOGICAL CHEMISTRY
Vol. 278, No. 44, Issue of October 31, pp. 43443–43451, 2003

Printed in U.S.A.

Solution Structure of the 162 Residue C-terminal Domain of Human Elongation Factor 1Bγ*

Received for publication, June 9, 2003, and in revised form, July 21, 2003
Published, JBC Papers in Press, August 13, 2003, DOI 10.1074/jbc.M306031200

Sophie Vanwetswinkel‡, Jan Kriek§, Gregers R. Andersen¶‖, Peter Güntert, Jan Dijk§, Gerard W. Canters‡, and Gregg Siegal‡ ‡‡**

*From the ‡Leiden Institute of Chemistry, Gorlaeus Laboratory, University of Leiden, Einsteinweg 55, 2333 CC Leiden, The Netherlands, the §Department of Molecular Cell Biology, Sylvius Laboratory, Wassenaarseweg 72, 2333 AL Leiden, The Netherlands, the ¶Institute of Molecular and Structural Biology, University of Aarhus, Gustav Wieds Vej 10C, 8000 Aarhus C, Denmark, and the **RIKEN Genomic Sciences Center, 1-7-22 Suehiro, Tsurumi, Yokohama 230-0045, Japan*

The multisubunit elongation factor 1 (eEF1) is required for the elongation step of eukaryotic protein synthesis. The eEF1 complex consists of four subunits: eEF1A, a G-protein that shuttles aminoacylated tRNAs to the ribosome; eEF1Bα and eEF1Bβ, two guanine nucleotide exchange factors, and eEF1Bγ. Although its exact function remains unknown, this latter subunit is present in all eukaryotes. Recombinant human eEF1Bγ has been purified and shown to consist of two independent domains. We have utilized high resolution NMR to determine the three-dimensional structure of the 19 kDa C-terminal fragment (domain 2). The structure consists of a five-stranded anti-parallel β-sheet surrounded by α-helices and resembles a contact lens. Highly conserved residues are mainly located on the concave face, suggesting thereby that this side of the molecule might be involved in some biologically relevant interface(s). Although the isolated domain 2 appears to be mostly monomeric in solution, biochemical and structural data indicate a potential homodimer. The proposed dimer model can be further positioned within the quaternary arrangement of the whole eEF1 assembly.

Elongation factor 1 (eEF1)[1] plays a central role in peptide elongation during the process of eukaryotic protein synthesis (reviewed by Merrick and Nyborg, Ref. 1). This multisubunit complex consists of two functionally distinct parts. eEF1A catalyzes the GTP-dependent delivery of aminoacylated tRNAs to the acceptor site of the ribosome. The eEF1B complex acts as an exchange factor (GEF) and recycles the inactive eEF1A-GDP released from the ribosome to the active GTP-bound state by stimulating nucleotide exchange on eEF1A. In metazoans, eEF1B is composed of three subunits, namely eEF1Bα, eEF1Bβ, and eEF1Bγ. Both the eEF1Bα and eEF1Bβ subunits promote *in vitro* nucleotide exchange reactions through a homologous C-terminal catalytic domain (2). The exact role of the third subunit, eEF1Bγ, is unknown. Unlike eEF1A and eEF1Bα (and eEF1Bβ), which are functional homologues of EF-Tu and EF-Ts in bacteria, eEF1Bγ is unique to eukaryotes. In fungi, eEF1B contains only eEF1Bα and eEF1Bγ.

Recent structural information has notably extended the understanding of the portion of the eukaryotic elongation cycle taking place away from the ribosome. After the initial solution structure of a catalytically active 91-residue GEF domain from human eEF1Bα (3) paved the way, a fuller picture of the nucleotide exchange mechanism was provided by analysis of the crystal structures of yeast eEF1A bound to the corresponding catalytic fragment of its exchange factor eEF1Bα, both in the absence and the presence of guanine nucleotides (4, 5). However, *in vivo*, the situation is much more complex with eEF1 in higher eukaryotes occurring as an assembly of at least four subunits. Based on various biochemical data, several models have been proposed for the quaternary organization of the eEF1 complex (6–10). Although presenting some discrepancies, all these models agree on the tight binding of eEF1Bα (and to a lesser extent eEF1Bβ) to eEF1Bγ through their respective N-terminal regions. Three of the models (7–9) also include the valyl-tRNA synthetase which is unique among the mammalian aminoacyl synthetases in its propensity to form a stable complex with eEF1 (11). Despite this extensive biochemical analysis, many questions about the function(s) of all of the eEF1 components remain unanswered. To extend our knowledge of the eEF1 organization and mechanism and shed light on the biological function of eEF1Bγ, we have focused in the present work on a structural study of this subunit.

Only scant information concerning the physiological function of eEF1Bγ is available. This subunit by itself is devoid of any exchange activity, but eEF1Bγ isolated from the brine shrimp *Artemia* stimulates the *in vitro* catalytic activity of the GEF eEF1Bα (12). Moreover, the protein was found to be poorly soluble in aqueous buffers and to co-purify and co-immunoprecipitate with tubulin. Based on these properties, Janssen *et al.* (12) proposed that this subunit might participate in directing components of the protein synthetic apparatus toward membranes and/or the cytoskeleton of the cell. Disruption of the two eEF1Bγ coding genes *tef3* and *tef4* present in the yeast genome

* This work was supported in part by the European Molecular Biology Organization through short-term fellowships (ASTF9702 and ASTF9809) (to S. V.). The costs of publication of this article were defrayed in part by the payment of page charges. This article must therefore be hereby marked "*advertisement*" in accordance with 18 U.S.C. Section 1734 solely to indicate this fact.

The atomic coordinates and structure factors (code 1PBU) have been deposited in the Protein Data Bank, Research Collaboratory for Structural Bioinformatics, Rutgers University, New Brunswick, NJ (http://www.rcsb.org/).

The chemical shift data reported in this paper have been submitted to the BioMagResBank Data Bank with the accession number(s) 5628.

‖ Supported by the Danish Science Research council.

‡‡ Recipient of Dutch Royal Academy of Sciences (KNAW) fellowship support. To whom correspondence should be addressed: Leiden Institute of Chemistry, Gorlaeus Laboratory, Einsteinweg, 55, 2333 CC Leiden, The Netherlands. Tel.: 3171-5274568; Fax: 3171-5274349; E-mail: g.siegal@chem.leidenuniv.nl.

[1] The abbreviations used are: eEF1, elongation factor 1; GEF, guanine nucleotide exchange factor; HMQC, heteronuclear multiple quantum coherence; HSQC, heteronuclear single quantum coherence; IPTG, isopropyl-1-thio-β-D-galactopyranoside; NOEs, nuclear Overhauser effects; NOESY, nuclear Overhauser enhancement spectroscopy; RMSD, root mean square deviation; UTR, untranslated region; DTT, dithiothreitol.

is non-lethal (13). The data currently available suggest that this subunit might be a regulatory element within eEF1B. The eEF1Bγ subunit is overexpressed in some gastric and esophageal carcinomas (14, 15) and is also a substrate for the cell cycle protein kinase CDK1/cyclinB (also known as maturation promoting factor, MPF) (16). Such phosphorylation may be part of a cell state-dependent regulation of the translation of valine-rich proteins as compared with other protein types (17). Furthermore, alteration of the level of eEF1Bγ encoding transcripts has been detected in mice tissues as a result of the onset of the aging process (18, 19). Very recently, eEF1Bγ was identified as capable of binding a highly conserved element within the 3′-UTR of vimentin mRNA using the yeast three-hybrid method (20). Additional complementary experiments performed on the endogenous as well as the recombinant human subunit extended this result to any type of RNA molecules tested, indicating thereby that eEF1Bγ is a nonspecific RNA-binding protein (Ref. 20).[2]

In order to gain further insight into the properties of this subunit, we have expressed recombinant human eEF1Bγ in *Escherichia coli*. In agreement with previous observations made on the *Artemia* eEF1Bα/eEF1Bγ complex (21), we found that the human eEF1Bγ is comprised of two trypsin-resistant, independently folding domains, namely a glutathione *S*-transferase-homologous N-terminal region (domain 1, ~25 kDa) responsible for the interaction with eEF1Bα and a highly conserved, exceptionally protease-resistant 162 residue C-terminal part (domain 2, eEF1Bγ-(276–437)). The domains are connected through a lysine-rich linker of about 45 residues. Here we present the high-resolution NMR structure of domain 2, which consists of a five-stranded, anti-parallel β-sheet surrounded by five α-helices. Analysis of our data in conjunction with previous reports suggests a homodimeric model for the eEF1Bγ subunit. Implications in terms of the quaternary organization of the entire eEF1 complex are discussed.

EXPERIMENTAL PROCEDURES

Protein Expression and Purification

Expression and Purification of Full-length eEF1Bγ—A plasmid carrying the gene coding for human eEF1Bγ fused to an N-terminal His_{10} tag (pET16b/eEF1Bγ) was transformed into the *E. coli* expression strain BL21(DE3). Bacteria were grown at 37 °C in LB medium containing 100 mg/liter carbenicillin.

Target protein expression was induced by addition of 0.7 mM IPTG to mid-log phase cultures ($OD_{600} \cong 0.6$). After 3.5 h of additional growth, bacteria were harvested by centrifugation. The pellet was resuspended in a buffer containing 40 mM Tris-HCl, pH 7.5, 5 mM $MgCl_2$, 150 mM KCl, 5 mM β-mercaptoethanol, 1 mM phenylmethylsulfonyl fluoride, and stored at −80 °C. Thawed cells were disrupted by sonication and debris spun down at 18,500 rpm, 4 °C for 2 h in a Beckman J2-MC centrifuge using a JA-20 rotor. After adjustment of pH to 7.5 and addition of imidazole and KCl to a final concentration of 5 mM and 0.5 M, respectively, the supernatant was applied to a HiTrap Chelating resin (Amersham Biosciences) charged with Ni^{2+} ions. The column was washed with 20 mM imidazole in 20 mM Tris-HCl, pH 7.5, 0.5 M KCl, and the protein was then eluted using 500 mM imidazole in the same buffer. Full-length eEF1Bγ was optionally further purified on Superdex 200 (Amersham Biosciences) using 20 mM Hepes pH 7.2, 350 mM KCl, 1 mM dithiothreitol, dialyzed into the appropriate buffer and concentrated in an Ultrafree-0.5 cartridge (Biomax-10, Millipore).

Preparation of eEF1Bγ Domain 2 Fragment by Limited Proteolysis—The full-length protein was prepared as above except that for isotopic labeling cells were grown in M9-based minimal medium supplemented with trace levels of metal ions and vitamins plus 0.3 g/liter $^{15}NH_4Cl$ and either 2 g/liter $^{13}C_6$-glucose or 4 g/liter unlabelled glucose (in the case of the 10% ^{13}C-labeled sample, a 1:10 mixture of labeled and unlabeled glucose was used). Moreover, bacteria were allowed to grow for 5 h instead of 3.5 after induction with IPTG.

eEF1Bγ-containing fractions obtained from the Ni^{2+} column were pooled and incubated on ice with trypsin (1/20, w/w, A grade, Calbiochem). After 2 h, the reaction was stopped using aprotinin (1:20, w/w, Merck) The crude proteolysis mixture was diluted with 4 volumes of cold water, dialyzed against 20 mM Tris-HCl, pH 7.5, 50 mM KCl, 5 mM β-mercaptoethanol, and loaded onto a SourceQ column (Amersham Biosciences) equilibrated in the same buffer at 4 °C. The domain 2 fragment was eluted using a 0.05–0.6 M KCl gradient. The protein was then dialyzed against the same buffer now containing 40 mM KCl in order to lower the salt content prior to concentration by reverse flow loading on a 1-ml Poros 20 HQ column. Further dialysis and concentration on Centricon MWCO 10 kDa (Millipore) yielded NMR samples containing ~1 mM of domain 2 in 20 mM Tris-HCl, pH 7.5, 75 mM KCl, 1 mM DTT to which 0.02% NaN_3 (w/v) and 5% D_2O (v/v) were added.

Preparation of eEF1Bγ Domain 1 Fragment—When necessary, the limited proteolysis conditions were adapted (lower trypsin concentration and shorter incubation time, to be tested for each different batch) to recover the fragment corresponding to domain 1 as well. The procedure used was the same as described above for domain 2 up to the point where the sample was loaded onto a SourceQ column (Amersham Biosciences). The domain 1 fragment was collected in the column flow-through, which was then diluted to adjust the buffer composition to 20 mM Tris-HCl, pH 7.8, 500 mM KCl, 5 mM imidazole, 5 mM β-mercaptoethanol. The sample was then loaded on a Ni^{2+}-charged HiTrap Chelating resin (Amersham Biosciences) 5-ml column. The column was eluted with 20 mM Tris-HCl, pH 7.8, 500 mM KCl, 5 mM β-mercaptoethanol containing 500 mM imidazole. Target protein fractions were pooled and dialyzed to obtain ~1.5 mg/ml samples in 20 mM Tris-HCl, pH 7.5, 75 mM KCl, 1 mM DTT, 0.02% NaN_3 (w/v).

Analytical Gel filtration and in Vitro Reconstitution Experiments—Analytical gel filtration was performed at room temperature on a Superdex 200 HR 10/30 column (Amersham Biosciences) equilibrated in 20 mM Hepes, pH 7.2, 350 mM KCl, 1 mM DTT. Samples containing 100–500 μg of protein(s) were centrifuged before loading on the column. The flow rate was 0.5 ml/min, and 0.5 ml fractions were collected. For reconstitution experiments, proteins were incubated together for 5 min on ice prior to loading.

Native Gel Electrophoresis and RNA Binding Bandshift Assays—Either poly(A) RNA (Roche Applied Science), poly(C) (Amersham Biosciences) or poly(U) (Roche Diagnostics) was dissolved in water to prepare a 10 mg/ml stock solution. Appropriate amounts were mixed with 3–5 μg of human recombinant eEF1Bγ or fragments thereof (Fig. 1*c*). The resulting mixtures were incubated for 15 min at 37 °C prior to loading on a 5% acrylamide gel run under native conditions.

NMR Spectroscopy and Resonance Assignment—All spectra were recorded at 25 °C either on Bruker DMX600, AV750 or Varian Inova 800MHz spectrometers. HNCACB (22), HBHA(CO)NH (23, 24), and CBCA(CO)NH (25), (26) were recorded for through-bond sequential backbone resonance assignment. Side-chain resonance assignments were mostly obtained from three-dimensional ^1H,^{13}C HCCH-TOCSY and CCH-TOCSY experiments (27). Aromatic ring proton and carbon resonance assignments were derived from the combined analysis of a two-dimensional ^{13}C,^1H CT (constant time) -HMQC spectrum (Fig. 2) (28, 29) and three-dimensional ^{13}C,^1H NOESY-HSQC (mixing time: 80 ms) plus HCCH-TOCSY spectra optimized for aromatic residue detection. Simultaneous analysis of three-dimensional ^{13}C,^1H NOESY-HSQC (mixing time: 80 ms), and ^{15}N,^1H NOESY-HSQC (mixing time: 150 ms) (30) spectra allowed confirmation and completion of the data. Except for this latter ^{15}N-edited NOESY spectrum, all experiments were recorded using a single double isotope-labeled sample. Prochiral methyl group stereospecific assignments were obtained by examination of the relative cross-peak sign in a two-dimensional ^{13}C,^1H CT-HSQC spectrum (28) recorded on a sample prepared from cells grown using 90% [$^{12}C_6$]glucose/10% [$^{13}C_6$]glucose (31).

Spectral data were processed using NMR-Pipe (32). Assignment and peak integration were performed using XEASY (33).

Structure Calculations—Structure calculations were performed with the program CYANA (www.guentert.com) using the CANDID method (34) for the automated assignment of the cross-peaks in the three aforementioned NOESY spectra. The final structure calculations with CYANA were started from 100 conformers with random torsion angle values. Simulated annealing with 10,000 time steps per conformer was performed with torsion angle dynamics (35) in CYANA. Restrained energy minimization of the 20 conformers with the lowest final CYANA target function values in a water shell using the AMBER force field (36) in the program OPALp (37) resulted in the solution structure of eEF1Bγ domain 2. The structure was validated using the program PROCHECK-NMR (38). Figures were generated with MOLMOL (39).

Data Bank Accession Number—The coordinates of the ensemble of 20

[2] W. M. Holmes and Z. F. Zehner, personal communication.

structures have been deposited in the RCSB Protein Data Bank (accession code 1PBU). Chemical shift data are available from the BioMagResBank under accession number 5628.

RESULTS

Characterization of Recombinant eEF1Bγ—The eEF1Bγ subunit of human elongation factor 1 (eEF1) carrying an N-terminal His tag was overexpressed in *E. coli*. The recombinant full-length protein was obtained in the soluble fraction and isolated in high yield (>20 mg/liter in LB medium) using metal affinity chromatography (Fig. 1*a*). When required, further purification was accomplished by size exclusion chromatography. Since the clone used carried a non-silent single point mutation in the eEF1Bγ coding gene (V289A) compared with the deposited sequence (NM_001404) (40), the integrity of the protein as well as its ability to form a complex with eEF1Bα were checked through analytical gel filtration techniques (data not shown). The three-dimensional structure indicates that this residue is surface exposed and is not part of a potential interaction interface providing further support that the mutation is not disruptive (see below). Unlike the equivalent protein isolated from the brine shrimp *Artemia* (12), the ~50 kDa recombinant human eEF1Bγ was found to be highly soluble with no tendency toward hydrophobic behavior. A possible explanation for this discrepancy is that isolation of the *Artemia* subunit required temporary treatment with denaturing agents that might have altered its biophysical properties. In contrast, purification of the recombinant human protein has been performed under conditions allowing the preservation of its native state.

Attempts to crystallize the full-length human eEF1Bγ failed. Limited proteolysis was then used to select for structurally stable domains (Fig. 1*a*). In agreement with previous observations made on the *Artemia* eEF1Bα/eEF1Bγ complex (21), we found that the human eEF1Bγ subunit is comprised of two trypsin-resistant domains of ~25 and 19 kDa respectively. Both domains were isolated independently and analyzed by a combination of *in vitro* reconstitution and gel filtration experiments (Fig. 1*b*). Whereas the full-length protein appeared to be either di- or trimeric (data not shown and Ref. 7),[3] each of the isolated domains was characterized by a retention time indicating that they were monomeric. While no interaction could be detected between them, the 25-kDa fragment (domain 1) was shown to bind eEF1Bα thereby indicating that it was derived from the N-terminal part of the intact protein (21). The smaller domain was identified as the C-terminal 162 residue fragment of eEF1Bγ (eEF1Bγ-(276–437, domain 2) based on Edman degradation sequencing and mass spectrometry data. This latter 19-kDa domain 2 turned out to be exceptionally resistant to further proteolysis, showing no sign of degradation after overnight incubation with trypsin (1:200 w/w, 0 °C) (Fig. 1*a*). Despite the unusually high stability and solubility properties demonstrated by the protein, only small plate-like crystals unsuitable for x-ray diffraction analysis could be obtained. On the other hand, the high level of dispersion evident in the one-dimensional ^{1}H NMR spectrum prompted us to elucidate its solution structure using NMR. In an attempt to simplify the purification procedure, the isolated domain 2 was cloned and overexpressed in *E. coli*. Rather unexpectedly, the protein was largely present in inclusion bodies. Although preliminary results indicated that the recombinant domain 2 could be solubilized and renatured, expression in M9-based minimal medium turned out to be very low. As a result, isotopic labeling, which is required for structural analysis by NMR, would have been too inefficient. We reverted therefore to the production of domain 2 by tryptic digestion of isotopically labeled full-length eEF1Bγ (^{15}N-labeled, ^{13}C,^{15}N-doubly labeled or 10% ^{13}C-labeled). NMR data were recorded for resonance assignment and structure determination.

It has recently been found that eEF1Bγ is a nonspecific RNA-binding protein (20) able to interact with poly(A) RNA.[2] In order to investigate, which domain of the intact protein is involved in RNA binding, we repeated these experiments using our recombinant, purified proteins. The full-length human eEF1Bγ subunit was shown to bind poly(A) RNA using an acrylamide gel-based band-shift assay performed under non-denaturing conditions (Fig. 1*c*). The assay indicates that there are several eEF1Bγ molecules bound to a single RNA molecule. No bandshift is observed for either domain 2 or domain 1 alone (Fig. 1*c*) suggesting that neither of the two domains is sufficient by itself for poly(A) RNA binding. Binding of the full-length protein has also been observed with poly(C) and poly(U) RNA (data not shown).

NMR Spectroscopy and Resonance Assignments—The high quality of the NMR data allowed us to obtain essentially complete ^{1}H, ^{13}C, and ^{15}N chemical shift assignments for the observable resonances (see Ref. 42), available from the BMRB under the accession number 5628 (42). Most of the backbone resonances were derived from combined interactive analysis of through-bond connectivities in triple resonance NMR spectra recorded on a ^{13}C,^{15}N-double-labeled sample and semiautomatic sequence-specific assignment using the program MAPPER (43). Of the 155 non-proline amino acids, there are only a total of six residues for which no backbone amide proton resonance could be identified (Lys-277, Asp-278, His-282, Phe-336, Asn-366, and Phe-384) and three of these are located at the N terminus. As is commonly found in NMR studies of proteins, the resonance of the HN proton of the first N-terminal alanine (Ala-276) could not be detected. Side-chain amide resonances could be identified for all of the seven Gln residues and four out of the six Asn residues. Stereospecific assignments of prochiral methyl groups were obtained for six of the seven Val residues and all fourteen Leu residues. Despite the unusually high number of aromatic amino acids contained in the protein sequence (3 His, 7 Trp, 7 Tyr, and 16 Phe), assignment of the aryl groups was completed to ~90%. An illustration of the complexity of the aromatic region is provided in Fig. 2, which presents the assigned two-dimensional ^{13}C,^{1}H CT-HMQC spectrum. The spectrum was recorded with a constant time period set so that the multiplicity of the carbons is indicated by the phase of the peak. However, not all of the aromatic proton and carbon chemical shifts could be identified for residues Phe-288, Phe-293, Phe-336, Phe-363, and Phe-423.

Unusual chemical shifts were observed for the backbone amide protons of Asp-315, Ala-383, and Phe-384 resonating at 3.80, 4.81, and 4.17 ppm, respectively. Significantly upfield-shifted resonances were also detected for some aliphatic side-chain protons of Ala-383 and Phe-384 as well as for Phe-314 and Gly-433. These chemical shift perturbations are likely to originate from strong ring-current effects due to the location of all of these residues within two aromatic clusters described below.

For 8 of 162 residues (Ser-338, Leu-341, Ile-342, Thr-343, Met-345, Gln-432, Gly-433, and Lys-434), a second backbone amide peak with intensity ~15% of the main peak could be unambiguously assigned based on triple resonance NMR experiments. In the case of Gly-433, we were moreover able to detect an additional weaker signal for the alpha proton resonances on the ^{13}C,^{1}H NOESY-HSQC. The same type of minor resonances have been assigned to Phe-346, Gln-347, Arg-348, and Ile-435 based on ^{15}N,^{1}H NOESY-HSQC pattern compari-

[3] M. G. Jeppesen, P. A. Ortiz, W. Shepard, T. G. Kinzy, J. Nyborg, and R. M. Andersen, submitted manuscript.

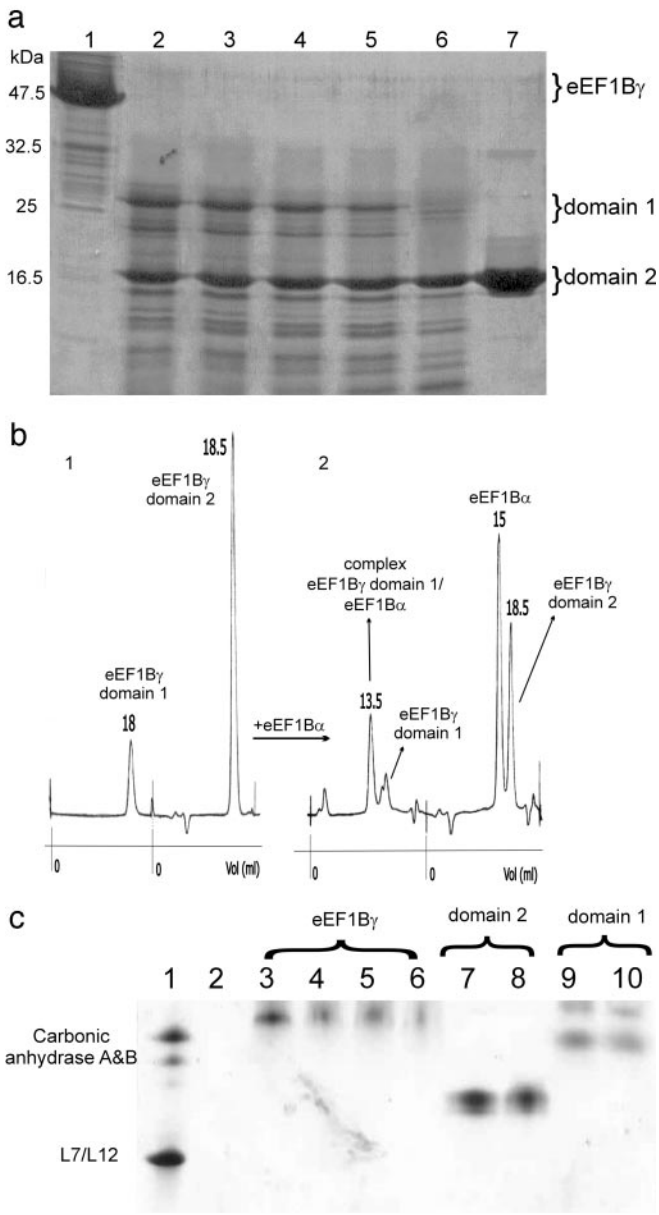

FIG. 1. **Biochemical characterization of eEF1Bγ.** *a*, SDS-PAGE (12.5% acrylamide gel) illustrating the high resistance of eEF1Bγ domain 2 to trypsinolysis. *Lane 1*, 5 μg of eEF1Bγ isolated by metal affinity chromatography; *lanes 2–6*, 10 μg of the same eEF1Bγ preparation after incubation on ice with 1:200 (w/w) trypsin (A grade, Calbiochem) for 1, 2, 3, 5 h and overnight, respectively; *lane 7*, domain 2 isolated using ion exchange chromatography. *b 1*, analysis of eEF1Bγ tryptic fragments by analytical gel filtration. Both domains were loaded at room temperature on a calibrated Superdex 200HR 30/10 column. The column was eluted at a rate of 0.5 ml/min, and the UV absorbance monitored at 280 nm. The elution volume (ml) of each peak is indicated. *b2*, *in vitro* reconstitution experiments. Both domains were incubated with ~0.8 equivalent of recombinant human eEF1Bα, incubated for 5 min on ice and loaded on the same Superdex column. In the case of the 25-kDa fragment, the chromatogram shows a peak shifted to the left indicating thereby the formation of a complex with its eEF1Bα partner. A smaller peak corresponding to the excess of eEF1Bγ domain 1 is observed as well. In contrast, incubation of the 19-kDa fragment with eEF1Bα yielded two peaks that elute at the respective positions of free eEF1Bα and free eEF1Bγ domain 2. *c*, bandshift assay: binding of eEF1Bγ to poly(A) RNA. *Lane 1*, molecular size indicators: 4 μg of *E. coli* ribosomal protein L7/L12 mixed with 2 μg of carbonic anhydrase (A and B, Sigma-Aldrich); *lane 2*, 210 pmol of poly(A) RNA (as nucleotide); *lanes 3–6*, 210 pmol of eEF1Bγ preincubated with 0, 0.03, 0.05, and 0.20 molar equivalent of poly(A) RNA, respectively. The addition of increasing amounts of poly(A) RNA leads to a reduction in the size of the band derived from free protein and the increased formation of large aggregates that do not enter the gel (not shown); *lane 7*, 210 pmol of domain; *lane 8*, 210 pmol of domain 2 preincubated with 1 molar equivalent of poly(A) RNA; *lane 9*, 100 pmol of domain 1; *lane 10*, 100 pmol of domain 1 preincubated with 2 molar equivalents of poly(A) RNA. In these latter cases addition of poly(A) RNA does not result in a change in the migration pattern of either domain 1 or 2.

son with the main signal. As sample homogeneity was confirmed by mass spectrometry, these extra peaks could derive from a minor species such as a homodimer of which a model is discussed below. Five additional weak $^{15}N,^{1}H$ HSQC peaks have been picked but could not be unambiguously identified. Possible assignments for these weaker peaks among the closest lying peaks from the main conformation were investigated. Two of the five peaks had likely resonance assignments that are consistent with the formation of a homodimer. However, three of these peaks cannot be directly explained by this model.

Structure Calculations and Quality of the eEF1Bγ Structure—The solution structure calculation was based on the analysis of nuclear Overhauser effects (NOEs) observed in a $^{15}N,^{1}H$ NOESY-HSQC and two $^{13}C,^{1}H$ NOESY-HSQC (optimized for aliphatic or for aromatic residues) three-dimensional spectra. Automated NOESY cross-peak assignments using the CANDID algorithm (34) implemented in the program CYANA resulted in the generation of an average of about 25 meaningful distance restraints per residue. Accordingly, the final structure calculation performed with CYANA was based on a total of 3920 meaningful interproton upper distance limits of which 33.5% are long range and 188 restraints for the backbone torsion angles ϕ and ψ that were derived from secondary $^{13}C\alpha$ chemical shifts (Table I). Structures were calculated using simulated annealing and torsion angle dynamics (35). Iterations of automated NOESY assignment and structure calculations followed by optimization of the input peak list were performed until the convergence criteria described by Hermann et *al.* (34) were met. The 20 final conformers with the lowest CYANA target function were retained for restrained energy refinement with OPALp (37). A best-fit superposition of the ensemble of the 20 lowest energy conformers is shown in Fig. 3*a*. The overall polypeptide fold is well defined with an average backbone RMSD to the mean of 0.46 Å. The statistics relating the structural parameters of the selected conformers that represent the solution structure of eEF1Bγ domain 2 are summarized in Table I.

Structure Description—Domain 2 of eEF1Bγ is a contact lens shaped molecule of approximate dimensions 51 × 43 × 32 Å that contains five α-helices and five β-strands (Fig. 3, *b* and *c*). The core of the molecule has the same fold as the catalytic domain of the eEF1Bα subunit with two α-helices and an anti-parallel four-stranded β-sheet (3, 4, 44). The resemblance is confirmed by a structure homology search using the Dali server (45). Moreover, this type of α/β fold is rather common and occurs frequently in ribosomal proteins and other elongation factors. The secondary structure elements, α-helices 3 and 5 and β-strands 1, 2, 3, and 5, form the core of the eEF1Bγ domain 2, whereas α-helices 1, 2, and 4 as well as β-strand 4 are packed around this core (Fig. 3*c*). The fourth β-strand runs anti-parallel to β-strand 1 and faces the convex surface of the lens that mainly contains loops connecting secondary structure elements. In contrast, the concave surface contains α-helices 1, 3, and 4 together with β-strand 5. The second α-helix forms one edge of the lens packing against α-helices 1 and 5. The remaining edges are mainly formed by loops especially at the N-terminal end, encompassing residues 276 to 289. The buried core of the molecule contains β-strands 1, 2, and 3.

Domain 2 contains an unusually high number of aromatic amino acids, about 20% of all residues. These residues pack together in two clusters, which are located on opposite faces of

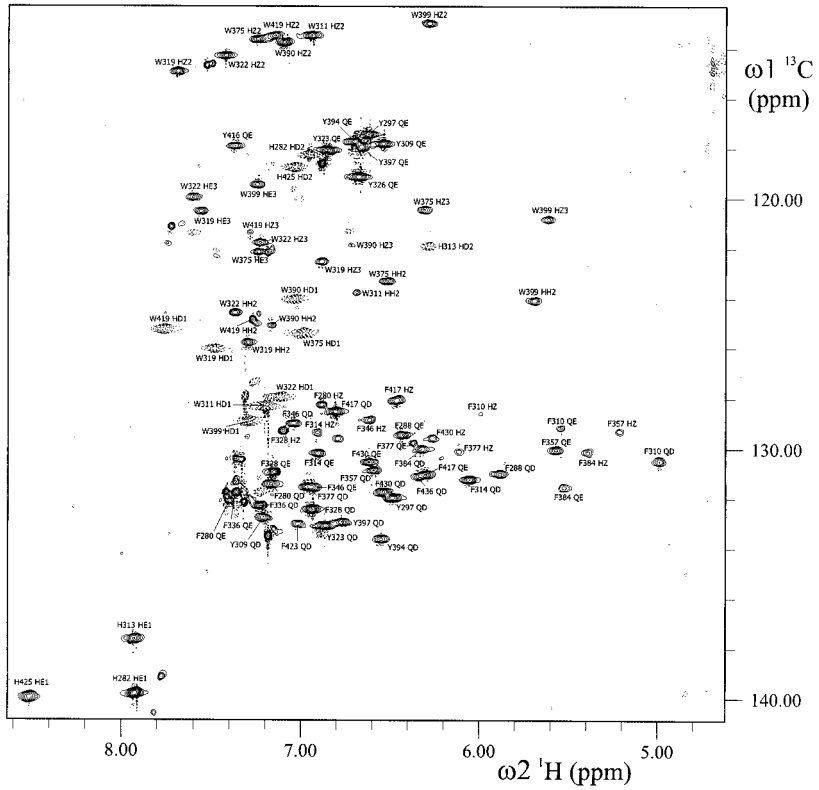

FIG. 2. **Two-dimensional ^{13}C,^{1}H CT-HMQC (28, 29) spectrum of recombinant human eEF1Bγ domain 2 acquired at 800 MHz, 298 °C and pH 7.5.** Peaks are identified by residue type (one letter code) and number followed by the assignment. Degenerate aromatic protons have been assigned the Q pseudo atom type. *Solid* and *dashed contours* correspond to signals due to aryl CH groups attached to an even or an odd number of carbon atoms, respectively.

TABLE I
Summary of structure statistics

Except for the number of restraints, average values given for set of 20 conformers with the lowest CYANA target function values (34, 35), after restrained energy-minimization in a water shell using the AMBER force field (36) in the program OPALp (37). The CYANA target function value is the average value for the 20 CYANA conformers before energy-minimization with OPALp.

NOE upper distance limits	
Total	3920
Intra residual and sequential ($\|i-j\|=1$)	1865
Medium range ($1<\|i-j\|<5$)	739
Long range ($\|i-j\|\geq 5$)	1316
Torsion angle restraints	188
CYANA target function value	1.83 Å^2
Distance restraint violations	
Number > 0.2 Å	0
Maximum	0.13 Å
Torsion angle restraint violations	
Number >5°	0
Maximum	3.97°
AMBER energies	
Total	−6207 kcal/mol
Van der Waals	−538 kcal/mol
Electrostatic	−6949 kcal/mol
RMS deviation from ideal protein geometry	
Bond lengths	0.0074 Å
Bond angles	1.89°
PROCHECK Ramachandran plot analysis (all residues)	
Residues in favoured regions	71.4%
Residues in additionally allowed regions	25.3%
Residues in generously allowed regions	2.4%
Residues in disallowed regions	1.0%
RMS deviation to the averaged coordinates	
Backbone atoms (276–437)	0.46 Å
Heavy atoms (276–437)	0.76 Å

the central β-sheet. Residues Phe-377 and Phe-384 form the center of the first cluster and are surrounded by Phe-280, Trp-322, Tyr-326, Trp-375, Trp-390, Tyr-397, Trp-399, and Phe-436. One function of this cluster may be to tightly anchor the long loop between strands β3 and β4 (residues 378–395) to the core of the protein. Associated with this first aromatic cluster, one finds a conserved salt bridge between Asp-315 and Arg-378 that in turn stacks against Trp-319 in what may be an amino-aromatic hydrogen bond (46, 47) as has been shown with the protein cutinase (48). This salt bridge links the loop between α-helix 2 and β-strand 1 in the core of the molecule to β-strand 4. The second aromatic cluster, centered around Phe-310, is surrounded by Phe-288, Phe-293, Tyr-297, Trp-311, Phe-314, Trp-319, and Phe-417. This latter cluster, which is remarkably well conserved, anchors α-helices 1 and 2 onto the core through interactions with α-helix 5 and β-strand 1.

The distribution of the surface-exposed, conserved residues in domain 2 is highly asymmetric. The concave surface and part of the edge surrounding it contain the majority of the conserved amino acids whereas the convex surface is relatively poorly conserved (Fig. 4). Exposed at the concave surface can be found both highly conserved charged and apolar (Phe-336, Met-337, and Trp-419) residues. Intriguingly, the strictly conserved C-terminal lysine, Lys-437, is solvent-exposed and both the side chain and the terminal carboxyl group contribute to the charge distribution of the concave surface. This situation resembles the essential function of Lys-205 and the terminal carboxyl group of Leu-206 in yeast eEF1Bα, which are both required for the nucleotide exchange reaction. Perhaps not surprisingly, the highly conserved residues on the concave face of domain 2 all lie within elements of regular secondary structure, while the non-conserved convex face is formed primarily by loops. Indeed, one would expect that the loop structure of the convex face would be more flexible in accommodating mutations that have occurred during evolution.

As part of the analysis of the structure of domain 2, we have calculated the charge distribution on the surface (Fig. 5*a*). There are two pronounced negatively charged patches on the surface of the molecule. One patch (Fig. 5*a*, *upper right*), located on the edge of the lens is almost strictly conserved and encompasses Glu-330, Glu-331, Asp-393, and Glu-395. A second patch (Fig. 5*a*, *lower right*), that is much less conserved, is

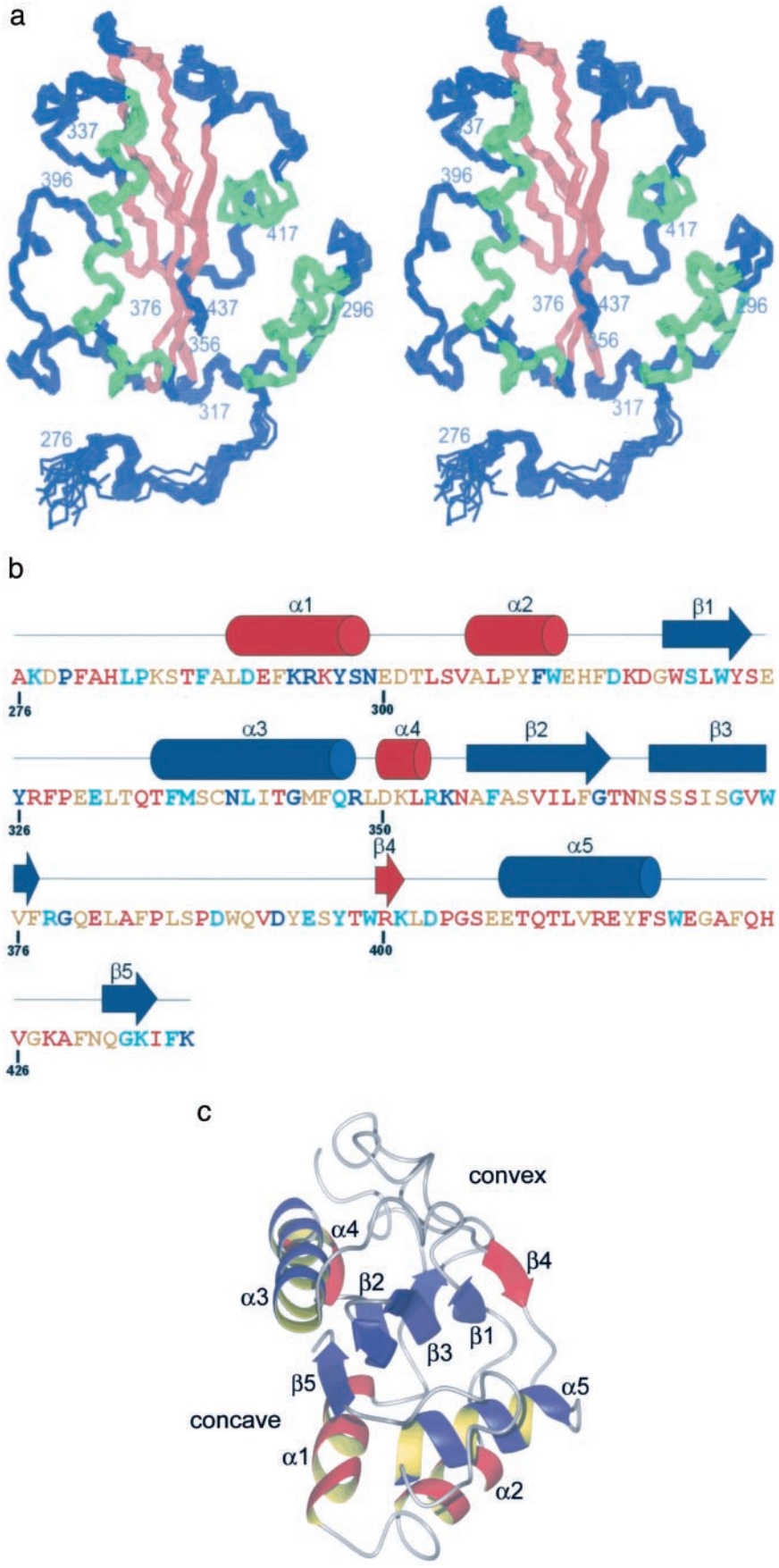

FIG. 3. **Topology and 3D structure of eEF1Bγ domain 2.** *a*, stereoview of the backbone (N, Cα, C′) of the best fit superposition of the final 20 selected conformers of human eEF1Bγ domain 2. The strands of the β-sheet are shown in *red*, the α-helices in *green*, and the loops in *blue*. *b*, sequence of human eEF1Bγ domain 2 colored according to an alignment of 21 representative sequences of orthologous proteins (SWISSPROT:

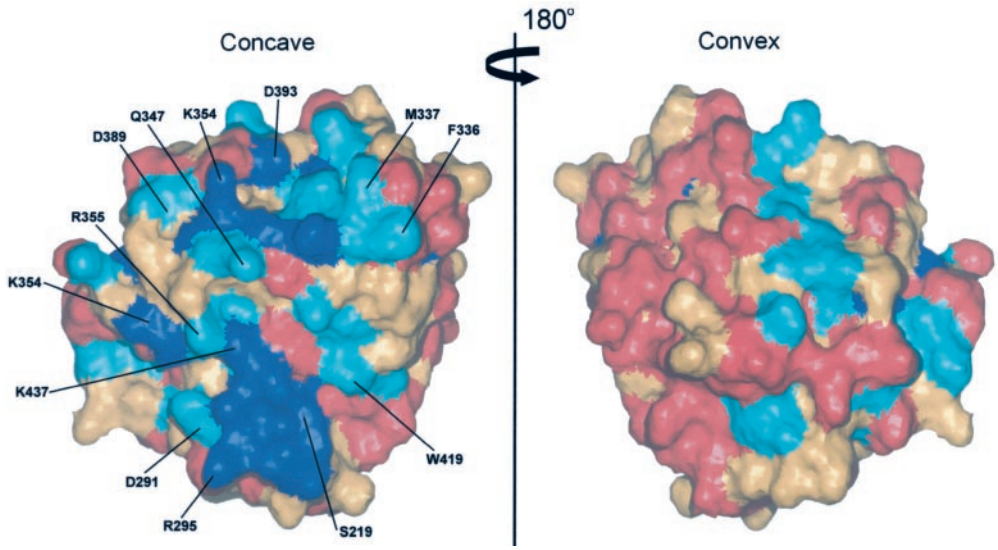

FIG. 4. **Residue conservation mapped onto the eEF1Bγ domain 2 surface.** Concave and convex faces are shown on the *left* and *right panel*, respectively. The residues are colored according to conservation as in Fig. 3*b*.

formed by Asp-403, Glu-407, Glu-408, Glu-415, Glu-420 and runs from the edge of the domain to its convex side. In contrast to these two negatively charged areas, the remaining negative and all the positive residues are scattered more or less randomly on the surface. We have also mapped the location of all twelve residues for which additional minor backbone NMR resonances have been assigned (see above). Interestingly, the majority of these residues are found in helix α3 and strand β5, which make up a large portion of the highly sequence-conserved, concave face of domain 2 (Fig. 5*b*).

DISCUSSION

The guanine nucleotide exchange factor eEF1B contains the catalytic subunits eEF1Bα and eEF1Bβ (the latter in metazoans only) in addition to eEF1Bγ. The function of the first two subunits has been demonstrated experimentally. In contrast, the cellular function of eEF1Bγ is not yet established. This subunit has previously been implicated in association with the ER, cytoskeletal elements and more recently, with RNA binding. However, deletion of both genes coding for eEF1Bγ in yeast is non-lethal and does not lead to severe effects on growth (13). Nevertheless, the eEF1Bγ subunit is present in all eukaryotes implying its involvement in a fundamental cellular process that is required under some yet to be defined conditions.

Our results confirm the earlier observations of van Damme *et al.* (21) that eEF1Bγ consists of two domains connected by a flexible linker. The N-terminal domain 1 is homologous to GST enzymes and maintains many features of the catalytic apparatus of these proteins (49, 50).[3] However, the overall level of conservation in domain 1 is intriguingly much lower than in domain 2 for which the high-resolution solution structure is described here. The high level of sequence conservation indicates that domain 2 is functionally important despite the fact that it is not required for the binding of either eEF1Bα or eEF1Bβ and is not sufficient by itself for RNA binding (Fig. 1*c*). Therefore, it seems likely that this domain of eEF1Bγ is involved in the quaternary organization of the entire eEF1B complex and/or in an interaction with a still unknown partner. However, in contrast to earlier suggestions (12), the very high solubility of recombinant human eEF1Bγ as observed in this study, makes it unlikely to interact directly with a hydrophobic environment such as in or at a membrane.

Although the isolated domain 2 is predominantly monomeric in solution, the intact eEF1Bγ appears to be a multimer. There are several observations supporting this. Analytical gel filtration experiments with both recombinant human and yeast eEF1Bγ indicate that the protein is organized as either a dimer or a trimer (data not shown).[3] The eEF1 complex purified from *Artemia* contains the four subunits eEF1A, eEF1Bα, eEF1Bβ, and eEF1Bγ in the ratio 2:1:1:1, but the eEF1Bβ-deficient complex eEF1A, eEF1Bα, and eEF1Bγ in the ratio 1:1:1, corresponding to the yeast eEF1 complex, was also observed. In both cases, experimental molecular mass determination indicated a dimeric state (10). Additional evidence for extensive multimerization of eEF1B is provided by the reported formation of dimers or trimers of eEF1Bα and eEF1Bγ in reconstitution experiments with recombinant rabbit subunits (7). Finally, the asymmetric unit of crystals of yeast eEF1Bγ domain 1 encompassing residues 1–219 contains a monomer, but a dimer organized around a crystallographic 2-fold axis is present in exactly the same arrangement as a dimeric GST enzyme. Also, a longer version of the same eEF1Bγ domain 1 is dimeric in solution suggesting thereby that residues 220–242 are required for dimerization to occur in solution.[3]

In principle, the eEF1Bγ subunit could dimerize entirely through its N-terminal GST-like domain. However, the extra set of NMR signals seen for a number of residues on the concave conserved face of domain 2 could be indicative of an equilibrium between a predominant monomeric and a minor

EF1H_YEAST; SWISSPROT:EF1G_YEAST; SWISSPROT: EF1G SCHPO; SWISSPROT:EF1G_ARTSA; SWISSPROT:EF1G_DROME; SWISSPROT:EF1G_XENLA; SWISSPROT:EF1G_RABIT; SWISSPROT:EF1G_HUMAN; SWISSPROT:EF1G_CAEEL; SWISSPROT: EF1G_TRYCR; SWISSPROT:EF1G_PRUAV; SWISSPROT:EF1G_ORYSA, SWISSPROT:EF1G_ARATH; GI:28922756; GI:18874390; GI: 12328430; GI:27545277; GI:15528538; GI:11228568; GI:13539556; GI:18958498) generated in ClustalW (Thompson *et al.*, 1994). The sequence represented here contains the mutation V289A (see text). The residue at this position is colored in the same way as the wild type would be. Residues identical in less than 50% of the sequences are shown in *red*, in less than 80% but at least 50% in *gold*, in less than 100% but at least 80% in *cyan*, and in 100% in *blue*. Also shown are the secondary structure elements (α-helices and β-strands) calculated in PROCHECK-NMR (38). Core and surrounding secondary structure elements are represented in *blue* and *red*, respectively. *c*, *ribbon diagrams* of eEF1Bγ domain 2 illustrating the lens shape of the domain. Secondary structure elements are colored as in Fig. 3*b*.

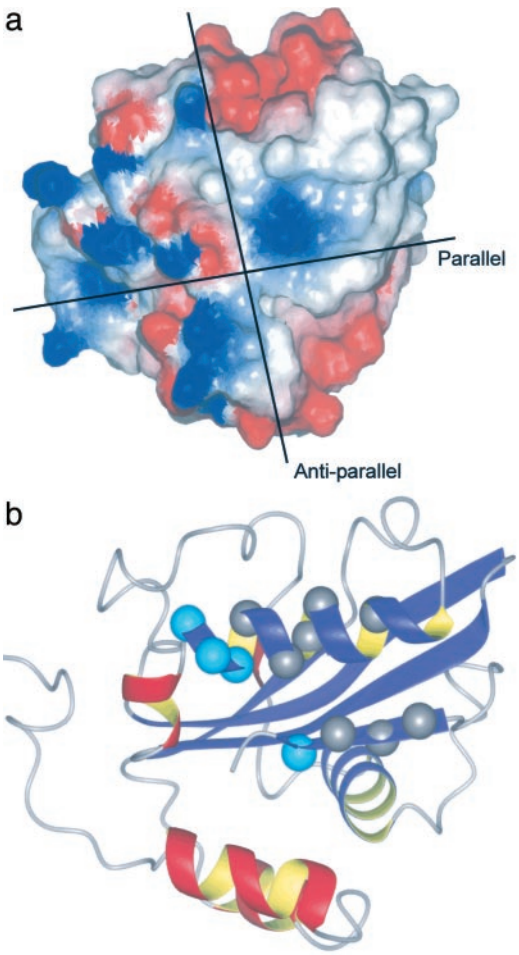

FIG. 5. *a*, the charge distribution (*red*, negative; *blue*, positive) on the concave surface of eEF1Bγ domain 2 oriented in the same way as in Fig. 4 (*left panel*). Orthogonal potential 2-fold "dimerization axes" (see "Discussion") are also shown. *b*, ribbon representation of eEF1Bγ domain 2. The molecule has the same orientation as in *panel a*. Residues for which additional minor backbone amide signals have been assigned on $^{15}N,^{1}H$ HSQC based on three-dimensional through-bond experiments are shown as *gray spheres* at the α carbon position. *Cyan spheres* represent residues for which the same type of minor resonances cannot be seen in three-dimensional through-bond experiments and therefore, tentative assignments have been made by comparison of the spin systems in a $^{15}N,^{1}H$ NOESY-HSQC. Note: *a*, except for the number of restraints, average values given for set of 20 conformers with the lowest CYANA target function values (34, 35), after restrained energy minimization in a water shell using the AMBER force field (36) in the program OPALp (37). The CYANA target function value is the average value for the 20 CYANA conformers before energy minimization with OPALp.

dimeric form. Alternatively, the extra set of peaks could also arrive from a slow internal conformational exchange mechanism, but this seems unlikely as a rather large portion of the protein would have to move with similar dynamics. Thus the simplest explanation is that the extra set of peaks derives from a different chemical or conformational environment experienced by these residues when domain 2 forms a homodimer. The coincidence in location between the peak doubling and the high level of sequence conservation is further support for the idea that this face is involved in dimerization. The putative dimer might be organized around a 2-fold symmetry axis running approximately parallel to the C-terminal β-strand 5 (Fig. 5*a*). Simple inspection of the structure shows that dimerization could then result in the formation of a large, intermolecular β-sheet consisting of 10 strands and that opposite charges could be matched across the interface (Fig. 5*a*). In this model, the two N termini of domain 2 would be close together in a parallel fashion and therefore be well suited to connect to the C-terminal ends of the GST-like domain 1 in the intact eEF1Bγ dimer. In the crystal structure of this latter domain, the C termini are also located in parallel. However, one could also imagine a dimer created by rotation around a 2-fold axis roughly perpendicular to β-strand 5. This could also lead to matching of opposite charges (Fig. 5*a*). But in the resulting complex, β-strand 5 and its symmetry-related mate would run in an anti-parallel fashion. A further result of this arrangement is that fewer residues are aligned to make intermolecular hydrogen bonds. Furthermore, the two N termini would lie on opposite sides of the dimer. Therefore we favor a parallel dimerization model. Our data fully agree with the model proposed for *Artemia* eEF1 (10) in which the four- as well as the three-subunit native complexes occur as dimers likely held together through eEF1Bγ. Since the individual domains are mostly monomers it seems likely that both domain 1 and 2 of the eEF1Bγ subunit are required for efficient stabilization of the entire assembly under physiological conditions. One should emphasize here that the putative dimerization of eEF1Bγ does not exclude any potential association of this subunit with other macromolecules. Association could happen either through occasional breakage of the suggested dimerization interface or involve another part of the surface. The former situation might be compatible with a competition phenomenon that could account for a hypothetical function of eEF1Bγ in the regulation of some cellular process(es).

eEF1Bγ has recently been reported to be a nonspecific RNA-binding protein (20). We confirmed this result for synthetic poly(A) RNA and extended it to poly(U) and poly(C) RNA. As none of the isolated domains can account by itself for this property, binding is likely to require the lysine-rich linker connecting the two eEF1Bγ domains. One could speculate about the biological relevance of this interaction that could anchor eEF1Bγ to the poly(A) tail of messenger RNAs and lead thereby to their co-localization with the elongation factor complex at the site of protein synthesis especially in the context of a end-to-end circularized mRNA complex (51). This would ultimately speed up the translation process in line with the channeling hypothesis that has been suggested for the protein biosynthetic machinery (41).

Acknowledgments—We thank Frans van Bussel for providing the pET16b/eEF1Bγ expression clone, Dr. Reinout Amons for Edman degradation sequencing, and Dr. Geerten Vuister for recording data at 800 MHz at the University of Nijmegen. We are also grateful to Prof. Antonie Maassen for his unconditional support and Dr. George Janssen for critical reading of the manuscript.

REFERENCES

1. Merrick, W. C., and Nyborg, J. (2000) in *Translational Control of Gene Expression* (Sonenberg, N., Hershey, J. W. B., and Mathews, M. B., eds) pp. 89–126, Cold Spring Harbor Laboratory Press, Cold Spring Harbor, NY
2. van Damme, H. T. F., Amons, R., Karssies, R., Timmers, C. J., Janssen, G. M. C., and Möller, W. (1990) *Biochim. Biophys. Acta* **1050,** 241–247
3. Pérez, J. M. J., Siegal, G., Kriek, J., Hard, K., Dijk, J., Canters, G. W., and Möller, W. (1999) *Struct. Fold. Des.* **7,** 217–226
4. Andersen, G. R., Pedersen, L., Valente, L., Chatterjee, I., Kinzy, T. G., Kjeldgaard, M., and Nyborg, J. (2000) *Mol. Cell* **6,** 1261–1266
5. Andersen, G. R., Valente, L., Pedersen, L., Kinzy, T. G., and Nyborg, J. (2001) *Nat. Struct. Biol.* **8,** 531–534
6. Mansilla, F., Friis, I., Jadidi, M., Nielsen, K. M., Clark, B. F. C., and Knudsen, C. R. (2002) *Biochem. J.* **365,** 669–676
7. Sheu, G. T., and Traugh, J. A. (1999) *Mol. Cell Biochem.* **191,** 181–186
8. Minella, O., Mulner-Lorillon, O., Bec, G., Cormier, P., and Bellé, R. (1998) *Biosci. Rep.* **18,** 119–127
9. Bec, G., Kerjan, P., and Waller, J. P. (1994) *J. Biol. Chem.* **269,** 2086–2092
10. Janssen, G. M. C., van Damme, H. T. F., Kriek, J., Amons, R., and Möller, W. (1994) *J. Biol. Chem.* **269,** 31410–31417
11. Motorin, Y. A., Wolfson, A. D., Orlovsky, A. F., and Gladilin, K. L. (1988) *FEBS Lett.* **238,** 262–264
12. Janssen, G. M. C., and Möller, W. (1988) *Eur. J. Biochem.* **171,** 119–129
13. Kinzy, T. G., Ripmaster, T. L., and Woolford, J. L. (1994) *Nucleic Acids Res.* **22,** 2703–2707
14. Chi, K. F., Jones, D. V., and Frazier, M. L. (1992) *Gastroenterology* **103,** 98–102

15. Mimori, K., Mori, M., Tanaka, S., Akiyoshi, T., and Sugimachi, K. (1995) *Cancer* **75,** 1446–1449
16. Janssen, G. M. C., Morales, J., Schipper, A., Labbé, J. C., Mulnerlorillon, O., Bellé, R., and Möller, W. (1991) *J. Biol. Chem.* **266,** 14885–14888
17. Monnier, A., Bellé, R., Morales, J., Cormier, P., Boulben, S., and Mulner-Lorillon, O. (2001) *Nucleic Acids Res.* **29,** 1453–1457
18. Lee, C. K., Weindruch, R., and Prolla, T. A. (2000) *Nat. Genet.* **25,** 294–297
19. Lee, C. K., Klopp, R. G., Weindruch, R., and Prolla, T. A. (1999) *Science* **285,** 1390–1393
20. Al Maghrebi, M., Brulé, H., Padkina, M., Allen, C., Holmes, W. M., and Zehner, Z. E. (2002) *Nucleic Acids Res.* **30,** 5017–5028
21. van Damme, H., Amons, R., Janssen, G., and Möller, W. (1991) *Eur. J. Biochem.* **197,** 505–511
22. Wittekind, M., and Mueller, L. (1993) *J. Magn. Reson. Series B* **101,** 201–205
23. Grzesiek, S., and Bax, A. (1993) *J. Biomol. NMR* **3,** 185–204
24. Wang, A. C., Lodi, P. J., Qin, J., Vuister, G. W., Gronenborn, A. M., and Clore, G. M. (1994) *J. Magn. Reson. Series B* **105,** 196–198
25. Grzesiek, S., and Bax, A. (1992) *J. Am. Chem. Soc.* **114,** 6291–6293
26. Muhandiram, D. R., and Kay, L. E. (1994) *J. Magn. Reson. Series B* **103,** 203–216
27. Kay, L. E., Xu, G. Y., Singer, A. U., Muhandiram, D. R., and Formankay, J. D. (1993) *J. Magn. Reson. Series B* **101,** 333–337
28. Vuister, G. W., and Bax, A. (1992) *J. Magn. Reson.* **98,** 428–435
29. Cavanagh, J., and Rance, M. (1993) *Annu. Rep. NMR Spectrosc.* **27,** 1–58
30. Pascal, S. M., Muhandiram, D. R., Yamazaki, T., Formankay, J. D., and Kay, L. E. (1994) *J. Magn. Reson. Series B* **103,** 197–201
31. Neri, D., Szyperski, T., Otting, G., Senn, H., and Wüthrich, K. (1989) *Biochemistry* **28,** 7510–7516
32. Delaglio, F., Grzesiek, S., Vuister, G. W., Zhu, G., Pfeifer, J., and Bax, A. (1995) *J. Biomol. NMR* **6,** 277–293
33. Bartels, C., Xia, T. H., Billeter, M., Güntert, P., and Wüthrich, K. (1995) *J. Biomol. NMR* **6,** 1–10
34. Herrmann, T., Güntert, P., and Wüthrich, K. (2002) *J. Mol. Biol.* **319,** 209–227
35. Güntert, P., Mumenthaler, C., and Wüthrich, K. (1997) *J. Mol. Biol.* **273,** 283–298
36. Cornell, W. D., Cieplak, P., Bayly, C. I., Gould, I. R., Merz, K. M., Ferguson, D. M., Spellmeyer, D. C., Fox, T., Caldwell, J. W., and Kollman, P. A. (1995) *J. Am. Chem. Soc.* **117,** 5179–5197
37. Koradi, R., Billeter, M., and Güntert, P. (2000) *Comput. Phys. Commun.* **124,** 139–147
38. Laskowski, R. A., Macarthur, M. W., Moss, D. S., and Thornton, J. M. (1993) *J. Appl. Crystallogr.* **26,** 283–291
39. Koradi, R., Billeter, M., and Wüthrich, K. (1996) *J. Mol. Graph.* **14,** 51–55
40. Kumabe, T., Sohma, Y., and Yamamoto, T. (1992) *Nucleic Acids Res.* **20,** 2598
41. Negrutskii, B. S., and Deutscher, M. P. (1991) *Proc. Natl. Acad. Sci. U. S. A.* **88,** 4991–4995
42. Vanwetswinkel, S., Kriek, J., Andersen, G. R., Dijk, J., and Siegal, G. (2003) *J. Biomol. NMR* **26,** 189–190
43. Güntert, P., Salzmann, M., Braun, D., and Wüthrich, K. (2000) *J. Biomol. NMR* **18,** 129–137
44. Kozlov, G., Ekiel, I., Beglova, N., Yee, A., Dharamsi, A., Engel, A., Siddiqui, N., Nong, A., and Gehring, K. (2000) *J. Biomol. NMR* **17,** 187–194
45. Holm, L., and Sander, C. (1993) *J. Mol. Biol.* **233,** 123–138
46. Burley, S. K., and Petsko, G. A. (1986) *FEBS Lett.* **203,** 139–143
47. Levitt, M., and Perutz, M. F. (1988) *J. Mol. Biol.* **201,** 751–754
48. Prompers, J. J., Groenewegen, A., VanSchaik, R. C., Pepermans, H. A. M., and Hilbers, C. W. (1997) *Protein Sci.* **6,** 2375–2384
49. Kobayashi, S., Kidou, S., and Ejiri, S. (2001) *Biochem. Biophys. Res. Commun.* **288,** 509–514
50. Kamiie, K., Nomura, Y., Kobayashi, S., Taira, H., Kobayashi, K., Yamashita, T., Kidou, S., and Ejiri, S. (2002) *Biosci., Biotechnol., Biochem.* **66,** 558–565
51. Wilkie, G. S., Dickson, K. S., and Gray, N. K. (2003) *Trends Biochem. Sci.* **28,** 182–188
52. Thompson, J. D., Higgins, D. G., and Gibson, T. J. (1994) *Nucleic Acids Res.* **22,** 4673–4680